




Original Article

Influence of anthropogenic activities on landslide susceptibility: A case study in Solan district, Himachal Pradesh, India

Sangeeta*  <https://orcid.org/0000-0001-8230-3299>;  e-mail: sangeeta546@gmail.com

S. K. SINGH  <https://orcid.org/0000-0001-6795-7294>; e-mail: sksingh@pec.edu.in

*Corresponding author

Department of Civil Engineering, Punjab Engineering College, Chandigarh 16012, India

Citation: Sangeeta, Singh SK (2023) Influence of anthropogenic activities on landslide susceptibility: A case study in Solan district, Himachal Pradesh, India. *Journal of Mountain Science* 20(2). <https://doi.org/10.1007/s11629-022-7593-1>

© Science Press, Institute of Mountain Hazards and Environment, CAS and Springer-Verlag GmbH Germany, part of Springer Nature 2023

Abstract: Landslides in the Himalayan region are primarily controlled by natural parameters, including rainfall, seismic activity, and anthropogenic parameters, such as the construction of large-scale projects like road development, tunneling and hydroelectric power projects and climate change. The parameters which are more crucial among these are a matter of scientific study and analysis. This research, taking Solan district, Himachal Pradesh, India, as the study area, aims to assess the impact of anthropogenic activities on landslide susceptibility at a regional scale. Landslide distribution was characterized into two groups, namely Rainfall-Induced Landslide (RIL) and Human-Induced Landslide (HIL) based on triggering factors. Multiple data such as slope angle, aspect, profile curvature, distance to drainage, distance to lineament, lithology, distance to road, normalized difference vegetation index (NDVI) and land use land cover (LULC) have been considered for delineating the landslide susceptibility zonation (LSZ) map. The effect of anthropogenic activities on landslide occurrences has been examined through the distribution of landslides along national highways and land use land cover changes (LULCC). Two sets of LSZ maps with a LULC of time interval covering five years (2017 & 2021) were prepared to compare the temporal progression of LULC and landslide susceptibility during the five

years. The results indicated the significant impact of anthropogenic activities on the landslide susceptibility. LSZ map of the year 2021 shows that 23% area falls into high and very high susceptible classes and 48% area falls into very low and low susceptibility classes. Compared to LSZ map of 2017, high and very high susceptible classes have been increased by 15%, whereas very low and low susceptible classes have been reduced by 7%. The present case study will help to understand the potential driving parameters responsible for HIL and also suggest the inclusion of LULC in landslide susceptibility analysis. The study will demonstrate new opportunities for research that could help decision-makers prepare for future disasters, both in the Indian Himalayan region and other areas.

Keywords: Landslide; Anthropogenic; Human-Induced Landslide (HIL); Rainfall-Induced Landslide (RIL)

1 Introduction

Landslide is a movement of a mass of soil (earth or debris) or rock down a slope (Couture 2011). Landslides can be initiated on slopes by natural causes (rainfall, snowmelt, changes in water level, stream erosion, earthquakes and volcanic activity) and man-made (disturbance by human activities like

Received: 04-Jul-2022

1st Revision: 19-Sep-2022

2nd Revision: 14-Nov-2022

Accepted: 30-Nov-2022

mining, construction and climate change) or any combination of these parameters. Landslides are severe geohazard and frequently occur in countries including China, Italy, Indonesia, Japan, the Philippines, the United States and Switzerland. Landslides also occur in many countries that straddle the Himalayas, like Nepal, Pakistan, and India. In the last two decades, approximately 4.8 million people have been affected and more than 18000 casualties have been reported due to landslides worldwide (Wallemacq et al. 2018).

Recent findings suggest that anthropogenic activities alter the topography (Ross et al. 2016). Many studies have reported that road construction and land use and land cover changes (LULCC) have a significant influence on landslide occurrences (Galve et al. 2015; Gariano et al. 2017; Guillard and Zezere 2012; Jones et al. 2021; Meneses et al. 2019; Tanyas et al. 2022). Climate change is bringing more extreme weather patterns, with heavy rainfall becoming more frequent. More landslides are expected to be triggered in the high mountain region due to climate change

(Merzdorf 2020). Many researchers have indicated the impact of anthropogenic activities and climate change on various parts of the world (Jones et al. 2021; Meusburger and Alewell 2008). Liu et al. (2021a) have indicated that there will be an increase in the occurrence of landslides in the high mountains of Asia due to anthropogenic activities and climate change.

In India, about 0.42 million km², or 12.6% of the land area is prone to landslide hazards. Out of this, 43% falls in North East (NE) Himalayas, 33% falls in North West (NW) Himalayas and 24% in the Western and Eastern Ghats (NIDM 2019). Due to complex physiography and increasing anthropological activities, Himachal Pradesh is recognized for frequent landslide occurrences, especially during the monsoon season. Rainfall-induced landslide of Kotrupi on August 13 2017 was one such devastating incident. At least 46 people lost their lives as two state transportation buses got buried under a massive landslide along National Highway (NH) 154. In 2022, three people were killed in a landslide at Menus in Simaur district of Himachal Pradesh. Earlier, in the year 2021, a massive landslide hit Himachal Pradesh, killing two persons while dozens were reported missing.

For the proposed research study, Solan district, Himachal Pradesh, India has been selected (Fig. 1). According to studies conducted in the past, landslide occurrence in Solan district, Himachal Pradesh has a wide distribution (Alsabhan et al. 2022; Panchal and Shrivastava 2022). The impact of landslides has largely increased recently due to the growth in population and expansion of civilization in hazard prone hilly terrain. Undoubtedly, much work on the geohazard has been done in this part of the

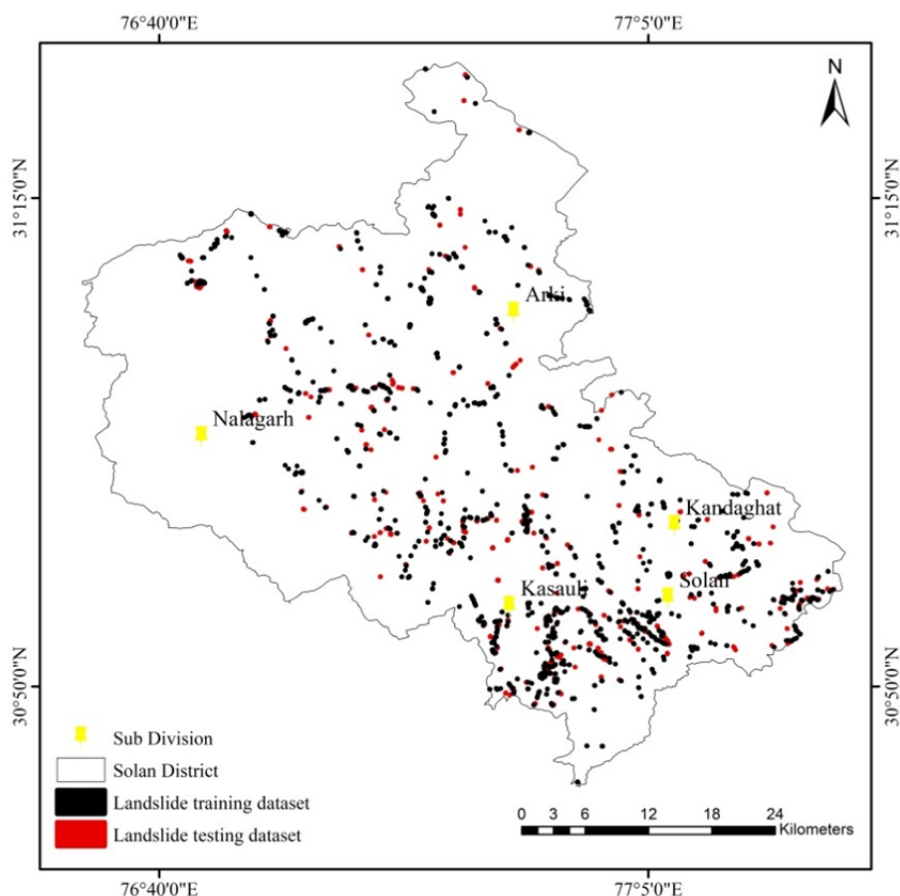


Fig. 1 Location map of the study area, Solan District, Himachal Pradesh, India.

Himalayas (Alsabhan et al. 2022; Nath et al. 2021; Panchal and Shrivastava 2021; Pandey et al. 2019; Pham et al. 2017; Sharma et al. 2020; Sharma and Prakash 2021; Sharma and Mehta 2012; Singh et al. 2021) but there is an absence of detailed information about the anthropogenic activities and climate change and how these factors impact occurrences of landslides. As many highways are under construction and many are in the planning phase in Himachal Pradesh which continuously interferes and destabilize the natural bed slope. Deforestation along the highway alignment also enhances the risk of landslides in Himachal Pradesh. Highway construction in mountainous regions significantly influences landslide occurrences (Chuang and Shiu 2018).

Various qualitative and quantitative approaches have been proposed to map landslide susceptibility areas in the literature (Kaur et al. 2017). Generally, four primary types of Landslide Susceptibility Zonation (LSZ) models are developed: expert-based (Ghosh and Bhattacharya 2010; Pradhan et al. 2017), statistical (Abdo 2022; Mehrabi 2022), machine learning (Akinci et al. 2021; Akinci and Zeybek 2021; Gao et al. 2021; Kundu et al. 2011; T. Liu et al. 2021b; Pourghasemi et al. 2021; Wan et al. 2021), and a hybrid model (Al-Najjar et al. 2021; Lv et al. 2022; Pradhan et al. 2021). Geographic Information System (GIS) techniques are beneficial in modeling landslide hazards using various statistical models (Sangeeta and Maheshwari 2022, Sangeeta et al. 2020; Saha and Saha 2021; Saranaathan et al. 2021; Wadadar and Mukhopadhyay 2022). In the present study Frequency Ratio (FR) method has been adopted to evaluate landslide susceptibility. FR is a bivariate statistical method that is widely used along with GIS to develop LSZ maps (Basu and Pal 2019; Saha et al. 2005). The relation between landslide incidence and landslide causative parameters can easily assess with the help of FR method (Vakhshoori and Zare 2016). Many studies have confirmed the accuracy of FR method is higher than other methods (Anbazhagan 2015; Ding et al. 2017; Gholami et al. 2019; Griffiths 2015; Huang et al. 2018; Nsengiyumva et al. 2018; Vakhshoori and Zare 2016). Recently FR based model has been used for LSZ mapping in many parts of the world by various researchers (Abdo 2022; Emadodin et al. 2021; Shano et al. 2021; Thomas et al. 2021).

Based on the increase in the frequency of landslides in changing the climatic regime, a novel

attempt to understand the influence of anthropogenic activities on landslide susceptibility in the Solan district, Himachal Pradesh, India has been made in this present research. For this purpose, the present study utilizes the statistical-based FR method. Various inherent landslide causative parameters, along with dynamic anthropogenic parameters have been used to prepare LSZ map. Spatial distribution of landslides has been categorized based on triggering parameters, i.e., Rainfall-Induced Landslides (RIL) and Human-Induced Landslides (HIL), to understand the behavior of anthropogenic parameters in landslide occurrence. A combined landslide inventory that is both RIL and HIL datasets have been used to develop LSZ map, whereas an individual sets of RIL and HIL were used to analyse the impact of anthropogenic activities on landslide occurrences. LSZ map of the year 2021 shows that 23% area falls into high and very high susceptible classes. Compared to LSZ map of 2017, high and very high susceptible classes have increased by 15%. Results indicate a significant impact of anthropogenic parameters on LSZ in the Solan district. This study will contribute to the scientific knowledge advancements on landslide phenomena. Developed GIS-based ready-to-use digital maps may assist planners in overall landslide hazard management.

2 Study Area and Methods

2.1 Study area

The study area is located in the Solan district, Himachal Pradesh, India. Fig. 1 shows the location of Solan district and landslide distribution. Solan district occupies an area of 1936 km² and encloses 76.42° and 77.20°E longitude and 30.05° and 31.15°N latitudes nestled on the lap of the Shivalik Ranges. Solan district lies in Seismic Zone IV, which is seismically very active. Solan district has high socio-economic importance from a tourism point of view and is known as Gateway to Himachal Pradesh as the NH 5 passes through this district. The altitude varies from 300 m to 3000 m (amsl). For Administrative purposes, the district has been divided into six sub-districts and five blocks. There are 240 panchayats in the district, covering 2614 villages.

2.2 Data, material and methods

The data types for various causative parameters

Table 1 Details of data and their sources

Thematic data	Resolution/Scale	Data source
Spatial distribution of landslide in polygon and point data	Google Earth, Published reports, GSI	Bhukosh portal, Geological Survey of India (GSI) http://bhukosh.gsi.gov.in/Bhukosh/Public
Elevation; Slope angle; Aspect; Profile Curvature	Cartosat 30 m	Bhuvan portal, National Remote Sensing Centre (NRSC) https://bhuvan.nrsc.gov.in/home/index.php
Distance to drainage	Digital Elevation Model (DEM), Cartosat 30 m	NRSC
Distance to lineament	Lineament map (1:25,000)	GSI
Lithology	Geological map (1:25,000)	GSI
NDVI	Landsat 8, 30 m	USGS earth explorer; https://earthexplorer.usgs.gov/
Distance to roads	Road network map	GSI
LULC	ESRI 10 m	https://www.arcgis.com/

and their resolution, scale and sources used in this study are the following (Table 1).

2.2.1 Landslide inventory

A landslide inventory is a detailed register of the distribution and characteristics of past landslides. In this study, the landslide records have been collected from the GSI Bhukosh portal. Landslide inventory is divided into two groups based on the triggering factor. One group is related to natural causes, i.e., rainfall. These landslides are referred to as Rainfall-Induced Landslides (RIL). Other landslides are induced due to human-related causes referred to here as Human-Induced Landslides (HIL). HIL are defined as landslides that are directly or partially triggered by anthropogenic activities like modification of the topography, changes in the water circulations, land-use changes and aging of infrastructure (Jaboyedoff et al. 2018). Combined landslide inventory which includes both RIL and HIL datasets, have been used to develop LSZ map. Further, separate datasets of RIL and HIL have been used for the impact assessment of anthropogenic activities on landslide occurrence. Landslide inventory map is given in Fig. 1. This inventory consists of 1030 landslides in the form of polygon data with a total of 1777 pixels. The largest aerial extent of a landslide is 122,000 m² and the smallest extent of 20 m². Landslides are also of varied types, involving different types of material and movement. Present landslide inventory contains 70% rock material and 30% debris material. 95% of landslides are slide movement and 5% have fall type of movement.

2.2.2 Landslide causative parameters and thematic layers preparation

The distribution of the landslides is significantly controlled by the topography, lithology, hydrology,

NDVI and anthropogenic activities. Therefore, estimating the influence of these causative parameters on the occurrences of the landslides is essential to understand their operating mechanism and to develop an LSZ map. The first step of the landslide susceptibility analysis is to determine the physical significance of the parameters to be used. To obtain a reliable map, the relation of each parameter with the landslide distribution must be evaluated using correlation and statistical distribution analyses. Discussion related to landslide causative parameters is given here.

(1) Topographic parameters

Spatial distribution of altitude is given by a digital elevation model (DEM). Surface topography controls flow direction & source, soil moisture and affect climate and vegetation, which are essential parameters that control landslide incidences (Ayalew and Yamagishi 2005). Fig. 2 shows the classified DEM for the Solan district. In Fig. 2(a), the whole area of Solan district has been classified into five classes in ascending order of elevation, whereas, Fig. 2(b) indicates the percentage area and percentage of landslides in each class. Landslide incidences are highest in the elevation range (1024–1423 m) (Fig. 2b).

(2) Slope angle

Slope angle is an essential causative parameter for landslide analysis and is used in preparing LSZ maps (Saha et al. 2005). DEM of 30 m resolution has been used to prepare a slope angle map using ArcGIS spatial analyst tool. The slope angle data is classified into six classes based on the steepness of the topography. Fig. 3(a) shows the slope angle map for the Solan district. Fig. 4(a) shows the landslides' spatial distribution in each slope angle class. The present study follows the trend, i.e., landslide

incidence increases with the increase of slope angle up to a certain angle, i.e., 25°–35°, where the maximum frequency of landslide is reached and then follows a decreasing trend. A similar trend was found by (Dai and Lee 2002). Fig. 4(a) shows that the highest landslide incidences are falling in the moderate class (25°–35°).

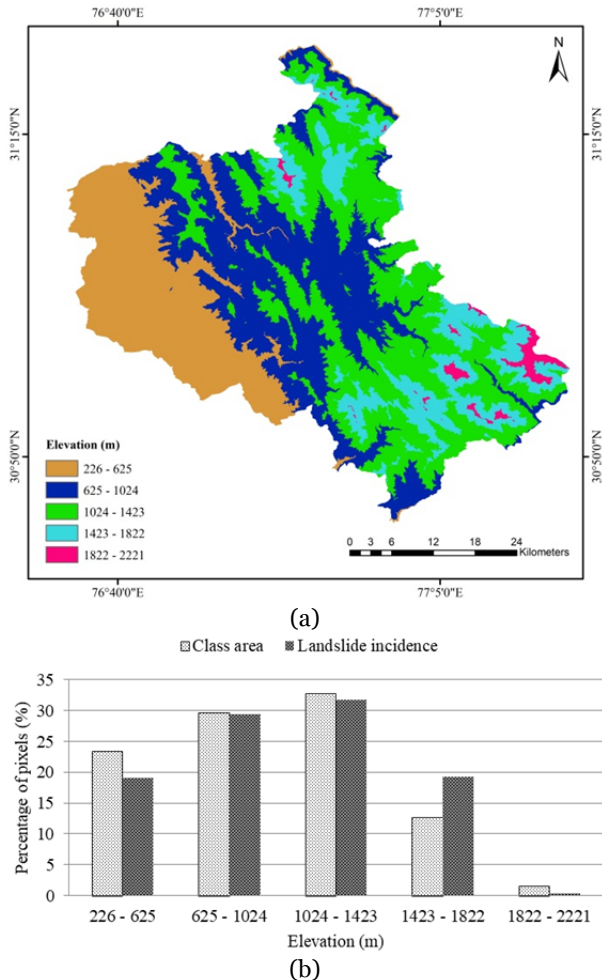


Fig. 2 DEM of the Solan district (a) Elevation map; (b) Spatial distribution of landslides in various elevation classes.

(3) Aspect

Landslide susceptibility is related to moisture retention and vegetation and controlled by the slope aspect. Fig. 3(b) presents the slope aspect map of Solan district. Slope aspect is categorized into ten directions. Literature shows that south-facing slopes are more vulnerable to landslides because the southern aspect, which receives excessive sun radiation and high rainfall, is more prone to landslides (Kumar and Anbalagan 2015). Fig. 4(b) shows that south-facing slopes, including southeast,

south and southwest contain the majority of landslides (48%), covering 38% of the study area.

(4) Profile curvature

Erosion and deposition are primarily controlled by acceleration and deceleration of flow, which is represented by curvature. The characterization of slope morphology and flow can be analyzed with the help of the general curvature map (Nefeslioglu et al. 2008). In general, the failure probability is higher for the concave morphology and this behavior is more evident as the slope increases (Giuseppe et al. 2016). Fig. 3(c) shows the slope curvature map of Solan district. Fig. 4(c) shows that 31% of landslides occurred in convex and highly convex classes, whereas 40% in concave and highly concave classes, i.e., landslides incidences are higher in the concave type of class.

(5) Distance to drainage

Distance to drainage is related to the pore water pressure in the slope, which significantly control the stability of the slope. Hence the distance to rivers was introduced as a critical causative parameter in previous research (Conoscenti et al. 2015; Pourghasemi et al. 2012; Shahabi et al. 2014). In this study, a drainage map with different orders of streams was extracted from 30 m DEM using the hydrology tool in ArcGIS. In this study, a buffer map with 250 m distance intervals to drainage has been prepared and classified into five categories, i.e., <250, 250–500, 500–750, 750–1000 & >1000. The drainage buffer map is shown in Fig. 3(d). Fig. 4(d) shows that 36% of landslides occurred <250 m.

(6) Distance to lineament

The lineaments represent structural discontinuities, which decrease the rock strength. Landslide frequency decreases with increasing distance from tectonic features (Saha et al. 2002). In Garhwal Himalayas, the effect of structural features on landslide incidences varies from 250 to 500 m (Saha et al. 2002). In the present study, the distance to lineaments map is classified into five classes with a 250 m interval (Fig. 3e). Fig. 4(e) shows that the majority of landslides (40%) fall in the first two classes, i.e., up to 500 m.

(7) Geological parameter: Lithology

Lithology is directly related to the landslide susceptibility of an area (Yalcin and Bulut 2007). The Solan district's spatial distribution of various lithological units is presented in Fig. 3(f). Rocks have some inherent properties like compactness,

composition & structure, which show different resistance against erosion and weathering. Fig. 4(f) shows the highest landslide incidences in Sirmur and Dharamshala groups.

(8) Anthropogenic parameter

The construction of buildings and roads in the region and deforestation are the anthropogenic parameters responsible for the landslide incidences (Kumar et al. 2018). To assess the impact of anthropogenic activities, three parameters, namely NDVI, distance to road and LULC have been taken in

the present study.

The NDVI is considered an influencing parameter in landslide susceptibility assessment as it estimates the vegetation density (Chen et al. 2017). NDVI map has been developed from Landsat 8 Operational Land Imager (OLI) imagery using Band 4 & 5. The vegetation cover represents the anthropogenic interference on hill slopes, which is related to landslide occurrences (Pradhan and Lee 2010). Fig. 3(g) shows the NDVI map of Solan district. Fig. 4(g) indicates that no vegetation, less vegetation and very

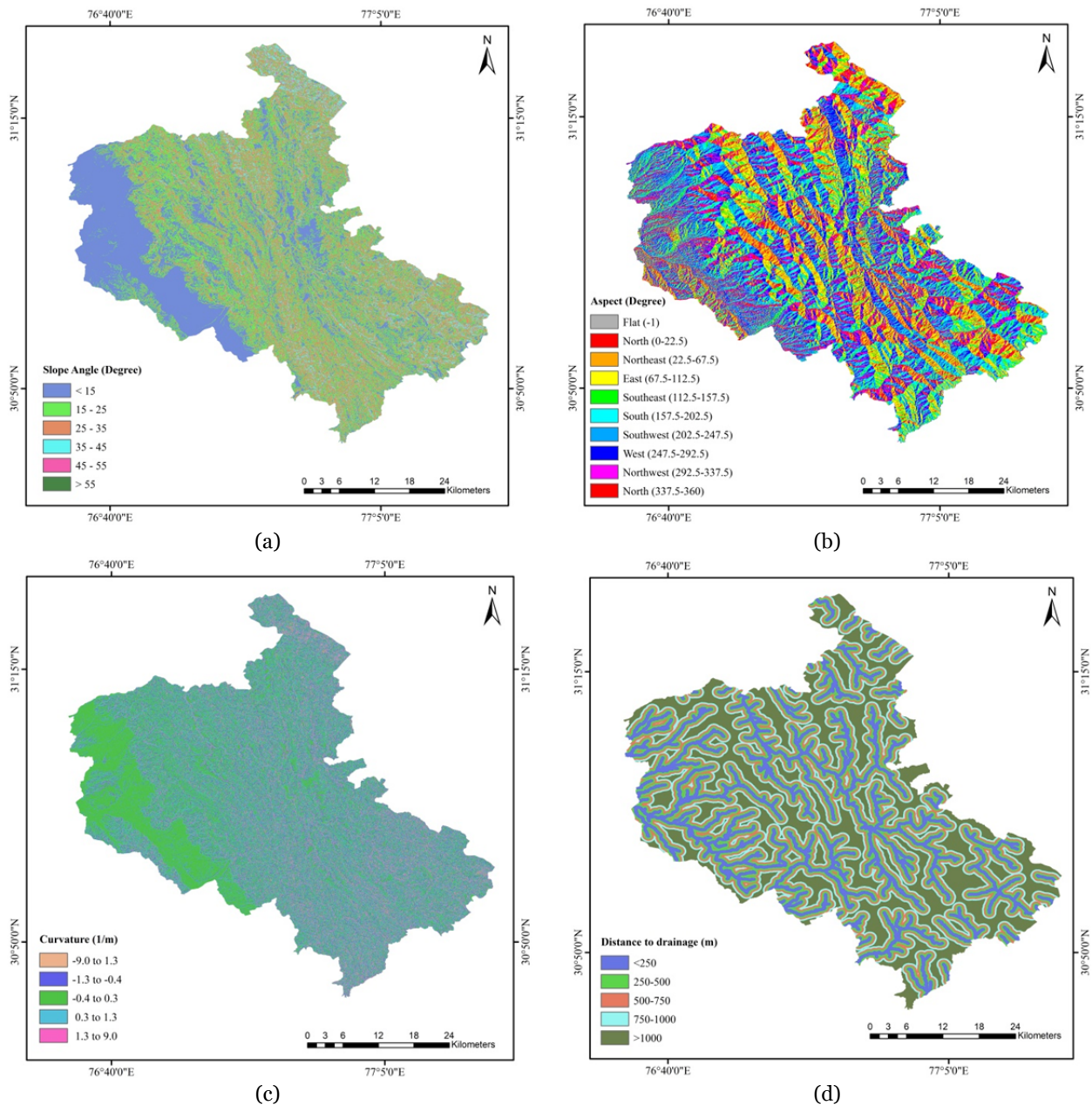


Fig. 3 Landslide causative parameters (a) Slope angle (b) Aspect (c) Profile curvature (d) Distance to drainage (e) Distance to lineament (f) Lithology (g) NDVI and (h) Distance to road. (-To be continued-)

(-Continued-)

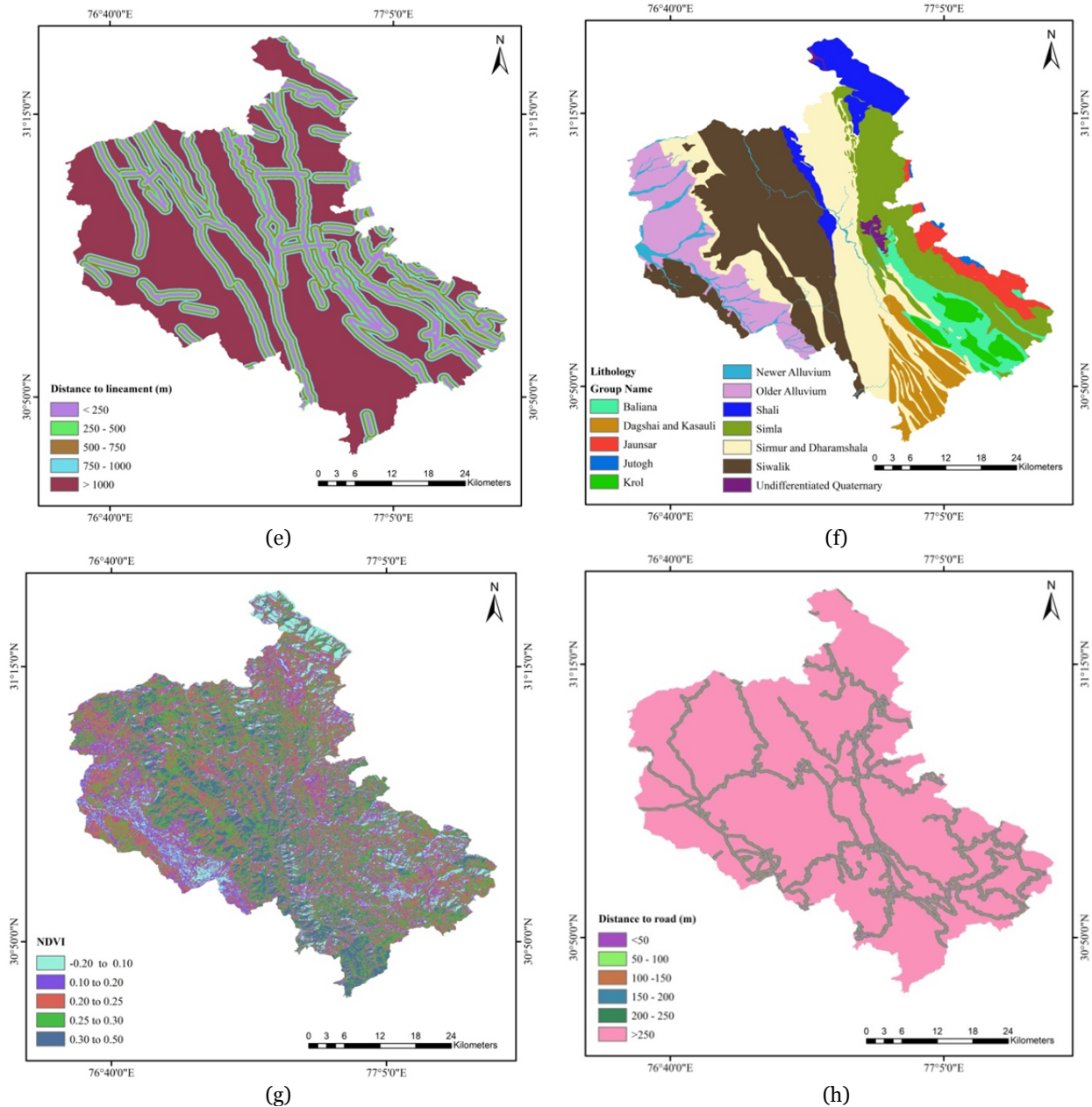


Fig. 3 Landslide causative parameters (a) Slope angle (b) Aspect (c) Profile curvature (d) Distance to drainage (e) Distance to lineament (f) Lithology (g) NDVI and (h) Distance to road.

less vegetation areas contain 69% of landslides.

The essential anthropogenic parameter causing landslides is road construction. The stability of Himalayan slopes has been, to a large extent, jeopardized by the construction of the road, which invariably involves steep and deep back cutting into hills. These cuttings include the tremendous release of stress, setting in the process of progressive failure. Mountainous areas have been experiencing extensive construction of road networks, housing development

schemes and expansion of existing road networks along with major river valley projects and tourism centers. All these activities have accentuated indiscriminate cutting of the slopes and made them vulnerable to failure. A road buffer map with buffer distances with an interval of 50 m was produced. Fig. 3(h) shows the distance to road in the Solan district. Fig. 4(h) indicates that 29 % of landslide incidences are <50 m.

Land use changes and their role in landslide

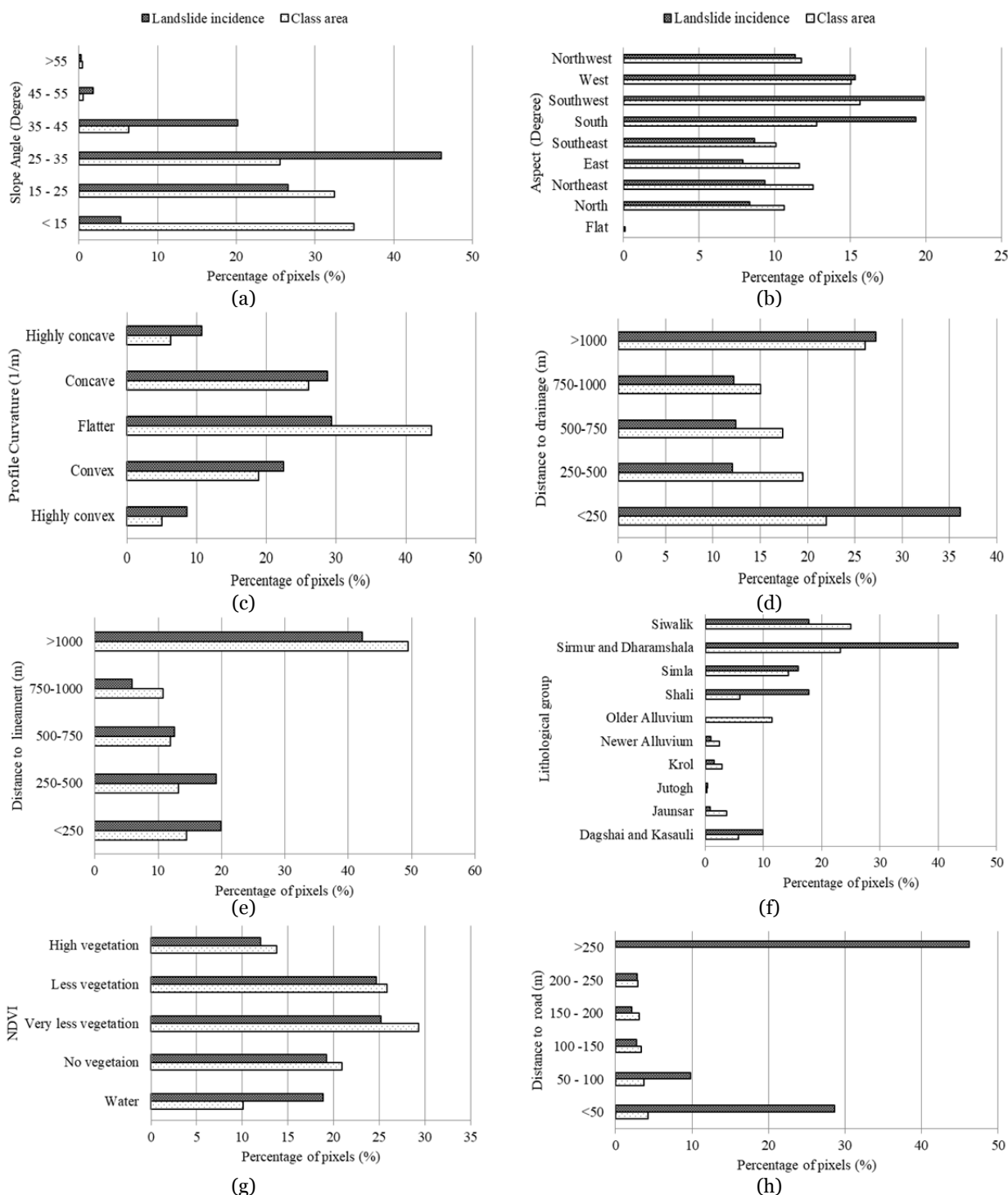


Fig. 4 Landslide incidence and class area details of causative parameters (a) Slope angle (b) Aspect (c) Profile of curvature (d) Distance to drainage (e) Distance to lineament (f) Lithology (g) NDVI and (h) Distance to road.

occurrences could be assessed by land use and land cover changes (LULCC). Many studies suggest that LULCC is responsible for landslide incidences (Galve et al. 2015; Guillard and Zezere 2012; Meneses et al. 2019). LULCC is more significant for initiating and re-

activating landslides in areas with high population density, infrastructure and human settlement (Abancó and Hürlimann 2014; Pinyol et al. 2012). The impact of LULCC on regional scale LSZ analysis has been illustrated by several researchers (Meneses et al.

2019; Pisano et al. 2017; Reichenbach et al. 2014). This study visualizes the LULC regarding water, trees, crops, built area, scrub and bare land and thus helps to assess the increasing exposure of landslide susceptibility. LULC maps for the years 2017 & 2021 are presented in Fig. 5. In the study area, the area covered by trees decreased by more than 12%, whereas crops, built-up, scrub and bare areas increased by about 2.04%, 12.46%, 32.68% & 39.11%, respectively. Landslide incidences have increased significantly in both built areas and bare land.

2.2.3 Adopted LSZ model: Formulation of Frequency Ratio (FR) method

Landslide distribution and landslide causative parameters have been utilized to calculate the FR using Eq. 1

$$FR_{i,j} = \frac{N_{i,j} / \sum_{j=1}^n N_{i,j}}{A_{i,j} / \sum_{j=1}^n A_{i,j}} \quad (1)$$

where $FR_{i,j}$ represents the frequency ratio of j^{th} parameter class of i^{th} parameter. $N_{i,j}$ is defined as a number of landslides in j^{th} parameter class of i^{th} parameter and $A_{i,j}$ is an area of j^{th} parameter class of i^{th} parameter. n represents the total number of parameter classes in a particular parameter.

Relative Frequency Ratio (RFR) has been utilized to normalize the FR values (Althuwaynee et al. 2016; Sifa et al. 2020). Eq. 2 has been adopted to evaluate the RFR values.

$$RFR_{i,j} = \frac{FR_{i,j}}{\sum_{j=1}^n FR_{i,j}} \quad (2)$$

The incorporation of parameter class weights (RFR_{ij}) was made in a weighted linear combination (WLC) model to estimate the landslide susceptibility index (LSI) for each pixel. WLC is a concept where event-causative parameters can be combined by applying primary- and secondary-level weights, as given in Eq. 3 (Ayalew et al. 2004). A classification technique proposed by Saha et al. (2005) was

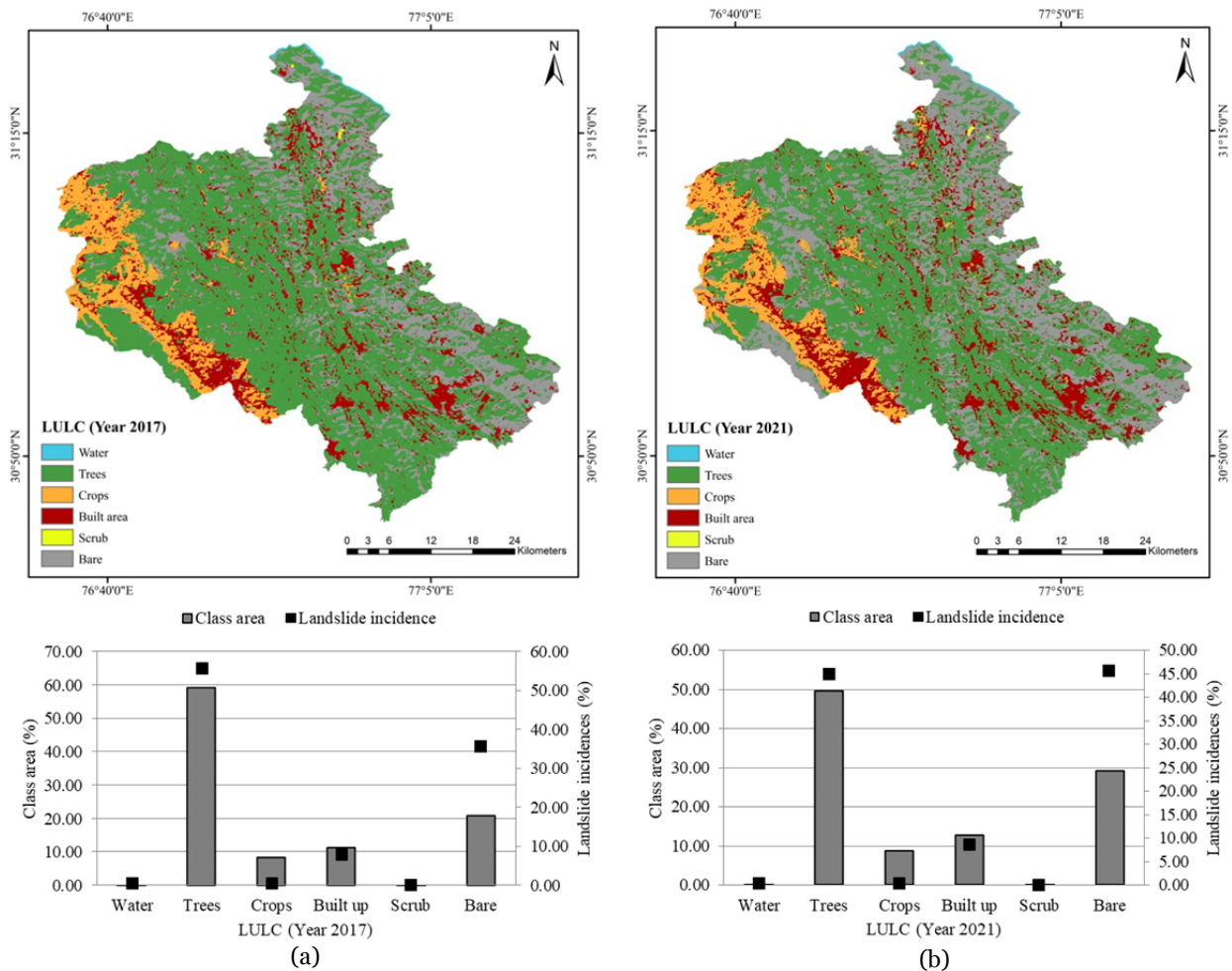


Fig. 5 LULC map of Solan district in 2017 and 2021.

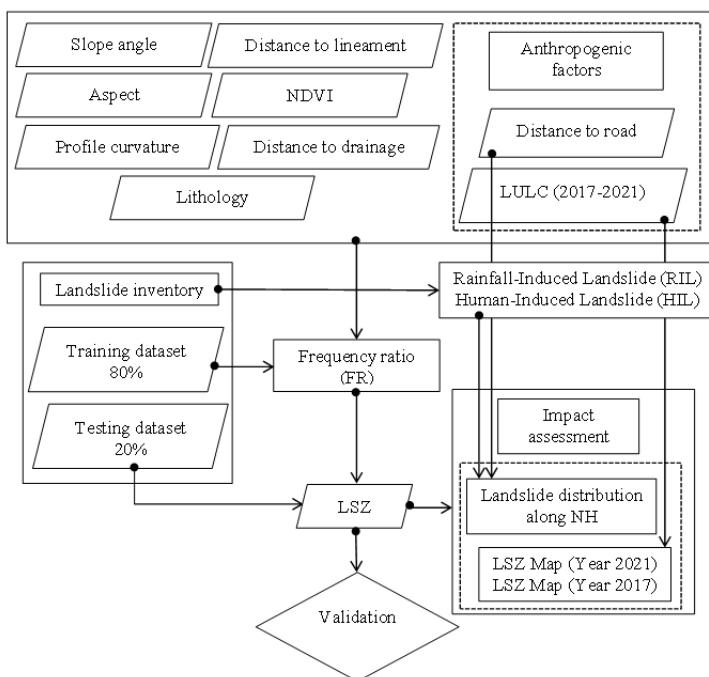


Fig. 6 Conceptual framework of the study.

incorporated to prepare the LSZ map of the study area. The flowchart of the present study is shown in Fig. 6.

$$LSI = \sum_{i=1}^m RFR_i \quad (3)$$

3 Results and Discussion

Using FR model, the landslide causative parameters were correlated with landslide inventory to determine the weightage for different causative parameter classes. The derived FR values and RFR for different parameter classes are presented in Table 2. Pixel-wise integration of these ratings (i.e., in terms of RFR values) has been performed to obtain LSI, and classification of the LSI values for the whole study area has produced the LSZ map.

Several classification schemes for LSI values are available in the literature, such as natural break, geometrical interval, quartile and standard deviation. In the present study, a method was proposed by (Saha et al. 2005). The mean (μ) and standard deviation (σ) of the LSI range has been calculated by the best-fit probability distribution curve. LSI values were classified into five susceptibility classes (ranges between very low to very high) with boundaries at $(\mu - 1.5\sigma)$, $(\mu - 0.5\sigma)$, $(\mu + 0.5\sigma)$ and $(\mu + 1.5\sigma)$. Here, m is defined as a number greater than zero (Saha et al. 2005). The m value rules the most

rational boundaries within the LSI. Different m values, i.e., 0.7, 0.8, 1.0 and 1.1 have been used to check the most appropriate LSZ map (Sangeeta and Maheshwari 2022). LSZ map was classified into five susceptibility classes namely Very Low Susceptible (VLS), Low Susceptible (LS), Moderate Susceptible (MS), High Susceptible (HS) and Very High Susceptible (VHS). LSZ map has been validated using training and testing datasets of inventories to evaluate their success and prediction rates, respectively.

3.1 FR and RFR calculation

Table 2 represents the calculation results of FR model for each class present in whole causative parameter maps based on the relationship with the training landslide inventory dataset. The RFR values were normalized from FR values between 0 to 1.

The relationship results in weights, which indicates the importance of factors/ classes on landslides. Topographic parameters are found to have a good relationship with landslide incidences. Among the slope angle categories, high RFR is observed in the very high slope category ($45^\circ - 55^\circ$). On steep slopes, the weight of the possible mobilized material under gravity will be more as compared to a moderate slope. Shear strength being the same in both cases, a steep slope with more mobilizing force may fail early (Anbalagan et al. 2015). Aspect is also found to be an important factor in this area. Very high RFR values, i.e., 0.12, 0.22 and 0.17 are found for the southeast, south and southwest aspects, respectively. Southern aspects of the study area, which receive excessive sun radiation and high rainfall, are more prone to landslides. In the case of drainage, RFR values are found to be high in the range of >250 m and it can be attributed to the stream bank erosion due to the river flow, such as gulling and toe cutting, which further leads to landslides (Anbalagan et al. 2015). The mapped lineaments significantly influence the spatial distribution of the landslides. Areas that are in close vicinity of the lineament show high RFR value. Lithology of the area belongs to different groups and each group is represented by a characteristic rock type, which might govern landslide incidence. Among different lithological units present in the study area, the Ballina group shows a high probability and has

Table 2 Spatial relationship between each landslide causative parameter and landslide

Landslide causative parameter	Class	Area (km ²)	A_{ij}	% of pixel in the class	L_{ij}	% of landslide pixels in the class	Training landslide pixels in the class		FR	RFR
							Number	%		
Slope angle (°)	< 15	675.33	797942	34.88	94	5.29	63	4.48	0.13	0.01
	15 - 25	627.77	741745	32.42	472	26.56	359	25.55	0.79	0.07
	25 - 35	493.56	583172	25.49	817	45.98	668	47.54	1.87	0.17
	35 - 45	121.51	143575	6.28	358	20.15	281	20.00	3.19	0.29
	45 - 55	9.66	11415	0.50	32	1.80	30	2.14	4.28	0.39
	>55	8.00	9876	0.43	4	0.23	4	0.28	0.66	0.06
Aspect	Flat	1.92	2263	0.10	0	0.00	0	0.00	0.00	0.00
	North	206.00	243055	10.62	148	8.33	93	6.62	0.62	0.08
	Northeast	242.41	286426	12.52	166	9.34	123	8.75	0.70	0.09
	East	224.83	265653	11.61	140	7.88	118	8.40	0.72	0.09
	Southeast	194.77	230131	10.06	154	8.67	130	9.25	0.92	0.12
	South	247.00	291844	12.76	343	19.30	304	21.64	1.70	0.22
	Southwest	302.00	356829	15.60	353	19.86	292	20.78	1.33	0.17
	West	290.57	343327	15.01	272	15.31	237	16.87	1.12	0.14
	Northwest	226.99	268198	11.72	201	11.31	108	7.69	0.66	0.08
Profile curvature	Highly convex	98.11	115927	5.07	154	8.67	127	9.04	1.78	0.28
	Convex	365.31	431628	18.87	399	22.45	323	22.99	1.22	0.19
	Flatter	846.40	1000066	43.71	522	29.38	420	29.89	0.68	0.11
	Concave	504.44	596024	26.05	511	28.76	383	27.26	1.05	0.16
	Highly concave	121.94	144080	6.30	191	10.75	152	10.82	1.72	0.27
Distance to drainage (m)	<250	425.65	502933	21.98	642	36.13	435	30.96	1.41	0.29
	250-500	377.83	446425	19.51	214	12.04	184	13.10	0.67	0.14
	500-750	336.83	397983	17.40	221	12.44	179	12.74	0.73	0.15
	750-1000	290.54	343285	15.01	217	12.21	179	12.74	0.85	0.18
	>1000	505.00	597100	26.10	483	27.18	428	30.46	1.17	0.24
Distance to lineament (m)	<250	56.09	333080	14.56	354	19.92	302	21.49	1.48	0.29
	250-500	55.76	302820	13.24	342	19.25	257	18.29	1.38	0.27
	500-750	55.57	273831	11.97	225	12.66	145	10.32	0.86	0.17
	750-1000	54.49	247693	10.83	105	5.91	79	5.62	0.52	0.10
	>1000	1714.00	1130301	49.41	751	42.26	622	44.27	0.90	0.17
Distance to road (m)	<50	81.92	96798	4.23	508	28.59	405	28.83	6.81	0.53
	50 - 100	72.34	85473	3.74	174	9.79	143	10.18	2.72	0.21
	100 -150	65.00	76796	3.36	49	2.76	39	2.78	0.83	0.06
	150 - 200	60.14	71059	3.11	38	2.14	30	2.14	0.69	0.05
	200 - 250	56.42	66659	2.91	51	2.87	43	3.06	1.05	0.08
	>250	1600.00	1890940	82.66	957	46.15	745	53.02	0.64	0.05
NDVI	Water	196.00	231422	10.12	335	18.85	196	13.95	1.38	0.26
	No vegetation	405.56	479195	20.95	342	19.25	290	20.64	0.99	0.19
	Very less vegetation	567.61	670661	29.32	448	25.21	377	26.83	0.92	0.18
	Less vegetation	501.00	591958	25.88	439	24.70	358	25.48	0.98	0.19
	High vegetation	266.17	314489	13.75	213	11.99	184	13.10	0.95	0.18
Lithology	Baliana	98.02	115815	5.06	144	8.10	136	9.68	1.91	0.19
	Dagshai and Kasauli	110.14	130135	5.69	175	9.85	140	9.96	1.75	0.17
	Jaunsar	69.27	81843	3.58	14	0.79	10	0.71	0.20	0.02
	Jutogh	5.17	6113	0.27	7	0.39	6	0.43	1.60	0.16
	Krol	55.12	65127	2.85	26	1.46	20	1.42	0.50	0.05
	Newer Alluvium	45.42	53670	2.35	17	0.96	14	1.00	0.42	0.04
	Older Alluvium	221.01	261131	11.41	0	0.00	0	0.00	0.00	0.00
	Shali	113.17	133717	5.84	315	17.73	22	1.57	0.27	0.03
	Simla	274.21	324406	14.18	283	15.93	237	16.87	1.19	0.12
	Sirmur and Dharamshala	447.50	528748	23.11	771	43.39	571	40.64	1.76	0.17
	Siwalik	484.33	572263	25.01	315	17.73	249	17.72	0.71	0.07
LULC (Year 2021)	Undifferentiated Quaternary	12.49	14757	0.65	0	0.00	0	0.00	0.00	0.00
	Water	5.56	6566	0.29	8	0.45	8	0.57	1.98	0.39
	Tress	957.11	1130871	49.43	815	45.86	647	46.05	0.93	0.18
	Crops	166.69	196950	8.61	7	0.39	7	0.50	0.06	0.01
	Built up	244.24	288583	12.61	135	7.60	105	7.47	0.59	0.12
	Scrub	1.24	1470	0.06	0	0	0	0.00	0.00	0.00
Bare	561.37	663285	28.99	812	45.69	638	45.41	1.57	0.31	

Note: A_{ij} , Number of pixels in the class; L_{ij} , Number of landslide pixels in the class. RFR, Relative Frequency Ratio.

the RFR value of 0.19. Building settlements over the slope play a main role in the landslide occurrences in the study area, which can be observed from the high frequency ratio for the built-up class in the LULC layer. In the study area, the road network has the highest influence on the spatial distribution of landslides with the highest FR. The area in the vicinity of 50 m buffer of the roads has the highest RFR of 0.53. This can be attributed to the fact that uncontrolled blasting and excavation during road construction on these fragile slopes lead to frequent landslides.

3.2 Classification of LSI and LSZ Mapping

The LSZ map of the study area using the RFR values of causative parameter classes pixel-wise has been generated using Eq. 1 & 2 and subsequently, the range of LSI values are classified into five different susceptibility classes. Two LSZ maps (Fig. 7) have been produced with the LULC data for the years 2021 and 2017, respectively. This study highlights the landslide susceptibility differences derived exclusively from the LULC data properties because the other landslide causative parameters are the same in both maps. A detailed discussion on the comparison and influence of anthropogenic activities on landslide susceptibility is presented in section 5.2. In the susceptibility map for the year 2021 (Fig. 7a), 6.07% of the total areas fall under the VHS class. The areas

categorized under HS, MS, LS, and VLS classes are found to be 16.48%, 29.15%, 30.70%, and 17.60%, respectively. The VHS class contains 38.36% area of the total landslide events and the VLS class contains only 0.57% area of the total landslide events. It is evident from Table 3 that the VHS classes of both training and testing datasets have the highest number of landslide incidences and lowest class area. The LSZ map is acceptable as higher percentages of landslide occurrence in the VHS class and a decreasing trend of class area have been observed toward higher susceptibility classes. LSZ map for the year 2021 shows that more area of VHS class falls in the built-up category as a comparison to LSZ map of the year 2017. In the LSZ map, VHS classes are concentrated along the road networks. These findings suggest the impact of anthropogenic activities on landslide susceptibility.

Table 3 Classification of landslide susceptibility zonation (LSZ) map in 2021

LSZ class	Landslide susceptibility index (LSI)	Area (%)	Landslide (%)	
			Training dataset	Testing dataset
Very Low	60 - 103	17.60	0.57	1.34
Low	103 - 121	30.70	8.11	5.65
Moderate	121 - 139	29.15	21.57	19.09
High	139 - 161	16.48	31.39	34.14
Very High	161 - 249	6.07	38.36	39.78

3.3 Verification and Validation of LSZ Map

In the current study, LSZ map produced by FR

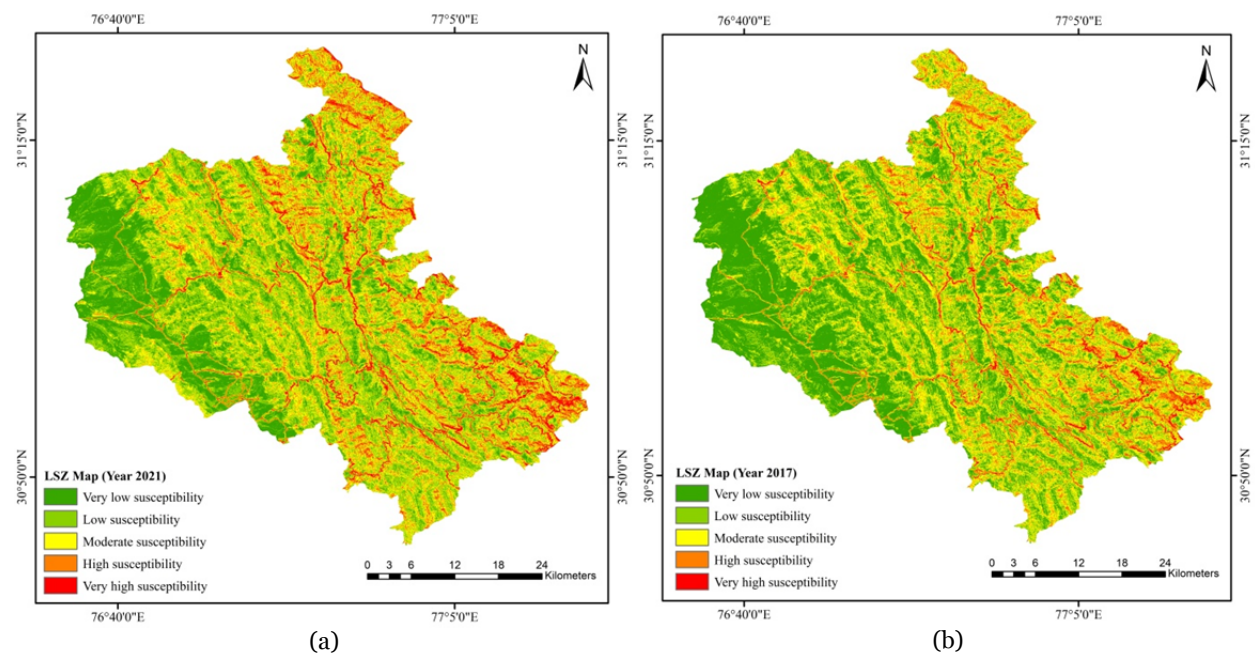


Fig. 7 Landslide susceptibility zonation (LSZ) maps of the Solan district in 2021 (a) and 2017 (b).

model was validated by comparing the LSZ map with the training and testing data sets. In order to do this, landslides were randomly separated into two data sets: 80% of landslides were classified as training data, and the remaining 20% of landslides were used as training data. Three different approaches, namely area under a curve, landslide density and root square mean error methods have been adopted.

3.3.1 Area under Curve

The area under curve (AUC) has been used to validate LSZ map of the year 2021 using success and prediction rate curves (Ozdemir and Altural 2013). Fig. 8 shows the Success and prediction rate curves for the study area. The success and prediction rate curve suggests that the AUC for the training and testing datasets are 0.79 & 0.80, which is a reasonably good value.

3.3.2 Landslide density

Landslide density has been utilized to verify the degree of fit of LSZ map of the year 2021. Landslide density is calculated using Eqs. 4(a, b).

$$\text{Landslide density}_{\text{training}} = \frac{\text{btr}_i}{a_i} \quad 4(a)$$

$$\text{Landslide density}_{\text{testing}} = \frac{\text{bts}_i}{a_i} \quad 4(b)$$

where training and testing landslides are presented by btr_i & bts_i , respectively and a_i is susceptibility class area. Table 4 shows the comparative results of landslide training and testing landslides. Landslide density for both training and testing data are comparable and maximum in VHS class, validating developed maps.

3.3.3 Root Mean Square Error

LSZ map of the year 2021 has also been validated through a statistical-based method, i.e., Root Mean Square Error (RMSE). RMSE is used to calculate the modeling error (Tsangaratos et al. 2017), which is calculated as follows:

$$\text{RMSE} = \sqrt{\frac{\sum_{i=1}^n (y_{\text{obs}} - y_{\text{pre}})^2}{N}} \quad (5)$$

where N is the number of landslides, y_{obs} is the observed landslide, and y_{pre} is the predicted landslide. According to Can et al. (2005), values of RMSE < 0.5 indicate good predictive models, respectively. In the present study, the result of RMSE is 0.056, confirming the model as a good predictive model for landslide susceptibility mapping.

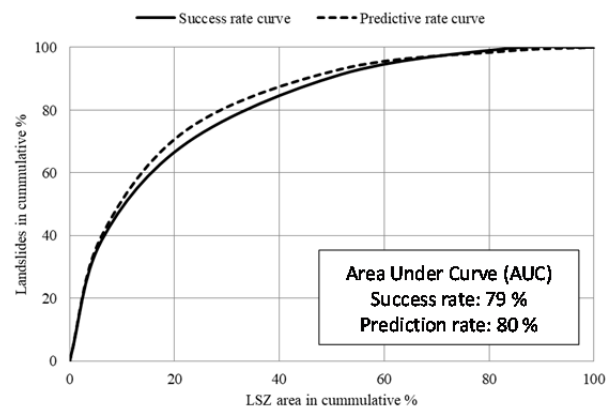


Fig. 8 Success and prediction rate curves of the landslide susceptibility zonation (LSZ) map.

Table 4 Landslide density for all landslide susceptibility zonation (LSZ) classes

LSZ Class	Landslide density	
	Training dataset	Testing dataset
Very Low	0.032	0.076
Low	0.264	0.184
Moderate	0.740	0.655
High	1.905	2.072
Very High	6.324	6.559

3.4 Impact of anthropogenic activities on landslide occurrences

An ever-growing inflow of tourists to towns and pilgrimages in the hills has led to a growing clamor for wider roads. However, the desire for quicker and easier access to the hills is coming at a high cost. Rampant widening of roads that pass through fragile mountains is leading to slope instability, irreparable damage to the ecology, and an increased risk of landslides. The impact of anthropogenic activities on landslide occurrences has been discussed here:

3.4.1 Landslide analysis along National Highways

Previous studies suggest landslide risk is associated with road construction (Agarwal and Dixit 1986; Arbanas and Dugonjić 2010; Gautam et al. 2019; Mukherjee et al. 2020). Road construction (new roads and road widening projects) is one of the main anthropogenic activities in the Himalayan region. Therefore, to understand the relationship between human-induced landslide (HIL) and road networks, the distribution of landslides along the four major national highways has been studied. Due to the width of the road network, in most cases, these infrastructures are included in the built-up area in

LULC map. So, understanding the individual impact of roads needs to be studied separately from the other anthropogenic activities. Fig. 9 shows the road network of the Solan district and landslide distribution along with it. A detailed analysis has been conducted to understand the landslide distribution along four major national highways, NH 5, NH 907A, NH 105 & NH 205 and their respective triggering mechanisms. A buffer of 1 km along the road has been created to analyze the landslide spatial distribution. Landslide inventory has been divided into two groups that are RIL and HIL to study anthropogenic activities. A total of 232 landslides are falling in the buffer zone, out of which 83 landslides are due to anthropogenic activities. Part of NH 5, which falls in Solan district, is 75 km long. A total of 151 landslides are falling in this

buffer zone. Out of this, 104 landslides are rainfall-induced and 47 are due to anthropogenic activities. This includes road widening and excessive settlement in the area. In recent years many landslides have been reported along national highways. According to studies conducted in the past, landslide occurrence in Solan district, Himachal Pradesh has a wide distribution, but there are a few pockets along NH 5, where slope failure is rampant and recurrent. These include Chakki Ka Mor, near Sanwara, Jabli, near Kumarhatti, Saproon Chownk, Dharampur. Fig. 10 shows some recent damage on NH 5.

NH 907A is a branch of NH 7. The length of NH 907A is 13.76 km. A total of 29 landslide events are reported along this highway, which are all rainfall-induced. Pinjore-Baddi-Nalagarh NH 21A is now known as NH 105. The total length of this highway in Solan district is 47 km. A total of 17 landslides are falling along this highway, and anthropogenic parameters trigger all. The total length of NH 205 is 38 km in the Solan district. A total of 35 landslides are falling along this highway. Out of 19 are anthropogenic and 16 are due to rainfall. Table 5 shows the recent landslides and damages along the national highways in Solan district. Results show that 36% of landslides along highways are triggered due to anthropogenic activities.

3.4.2 Evolution of LULC and LSZ

Two different LSZ maps have been prepared by LULC map for the years 2017 and 2021 to compare the temporal progression of LULC and landslide susceptibility for the duration of the last five years. Fig. 7(a) shows the LSZ map developed by LULC for the year 2021, which has been compared with the LSZ map for the year 2017 shown in Fig. 7(b). Results clearly depict the change in all susceptibility classes. Area of VLS & LS classes has decreased from the year 2017 to 2021. On the contrary, MS, HS and VHS classes have increased. The comparison between the LULC maps (Fig. 5) reveals that the area occupied by forest has reduced, whereas the area occupied by bare land increased. The present result confirmed the hypothesis that the susceptibility to landslides is dependent on the LULCC (Vanacker et al. 2003). Many previous studies have suggested that the frequency of landslides and associated risks to infrastructure buildings and people are likely to increase due to changing climate and land use patterns (Gariano and Guzzetti 2016). It is evident

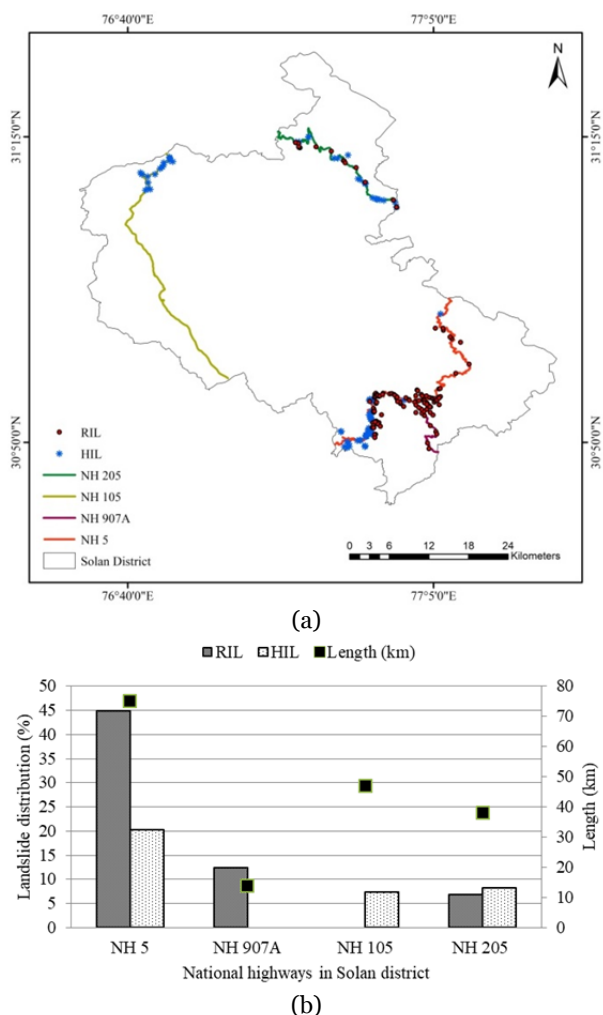


Fig. 9 (a) Rainfall-Induced Landslide (RIL) and Human-Induced Landslide (HIL) distribution; (b) Spatial distribution of landslides in various elevation classes along National highways in Solan district.



Fig. 10 Landslide damage on NH 5. (a) A portion of Parwanoo-Shimla road caved near Chakki Mod (Source: <https://indianexpress.com/article/india/landslides-disrupt-rail-and-road-traffic-between-chandigarh-and-shimla-5305537/>); (b) Big boulders often fall on the four-laned Parwanoo-Dharampur section (https://www.tribuneindia.com/news/himachal/single-lane-traffic-to-avert-mishaps-on-parwanoo-nh-301197).

Table 5 Recent landslide incidences in the Solan district

National Highway	Detail of landslide event	Date of event
NH 5	NH 5 was blocked due to a landslide in Kandaghat in the Solan district of Himachal Pradesh	Jul. 29, 2021
NH 907A	One person died and two others were injured due to the landslide, the Nahan-Kumharhatti NH-907-A was blocked	Aug. 4, 2021
NH 5	In a bid to avert accidents due to reoccurring landslides and shooting stones on the Parwanoo-Kaithlighat section of National Highway NH 5, vehicular traffic is channeled through a single lane	Aug. 24, 2021
NH 205	A massive landslide blocked the National Highway 205	Sep. 14, 2021
NH 5	Landslide near Kandaghat on the Solan-Shimla section of NH 5 caused a temporary halting of traffic	Nov. 24, 2021
NH 5	A landslide at Kyaribaglou near Kandaghat in Solan district caused major disruption on the Chandigarh-Shimla NH 5	Sep., 2020
NH 5	Massive mudslides hit the Chandigarh-Shimla national highway between Parwanoo and Solan towns in Himachal Pradesh	Jul. 13, 2019

from the LULCC maps that there is an increase in the built-up area. Population increase and infrastructure construction in the vulnerable zone are intensifying the probability of landslides. In the GIS-based method, the selection of high quality, accurate and up-to-date landslide controlling parameters, landslide inventory and appropriate analysis approach is very important (Magliulo et al. 2008). In the case of the Solan district, nine spatial landslides controlling parameter along with a detailed landslide inventory has been adopted to perform LSZ map. Comparing the LSZ maps of different time span shows the significant role of anthropogenic activities on landslide susceptibility. Fig. 7 clearly shows that areas around built-up areas and road networks fall in the HS and VHS classes. LSZ maps designate the most vulnerable areas in the Solan district, which may be the basis for the use of preventive or protective measures. Fig. 11 (a) shows the Spatial distribution of HIL, which has been used

to check the relation between anthropogenic activities and landslide susceptibility. Fig. 11 (b) clearly shows that more number of human-induced landslides is falling in the VHS class in the year 2021 as compared to 2017. This clearly confirms that area which is prone to landslides has been increased and influenced by anthropogenic activities.

4 Conclusions

The present study focuses on the influence of anthropogenic activities on landslide susceptibility zonation (LSZ) mapping in mountainous area. For this purpose, Solan district is chosen because it is an important location from a tourism point of view and there were a lot of landslides in the past. This study adopted a bivariate statistical-based frequency ratio (RFR) model to simulate the landslide susceptibility.

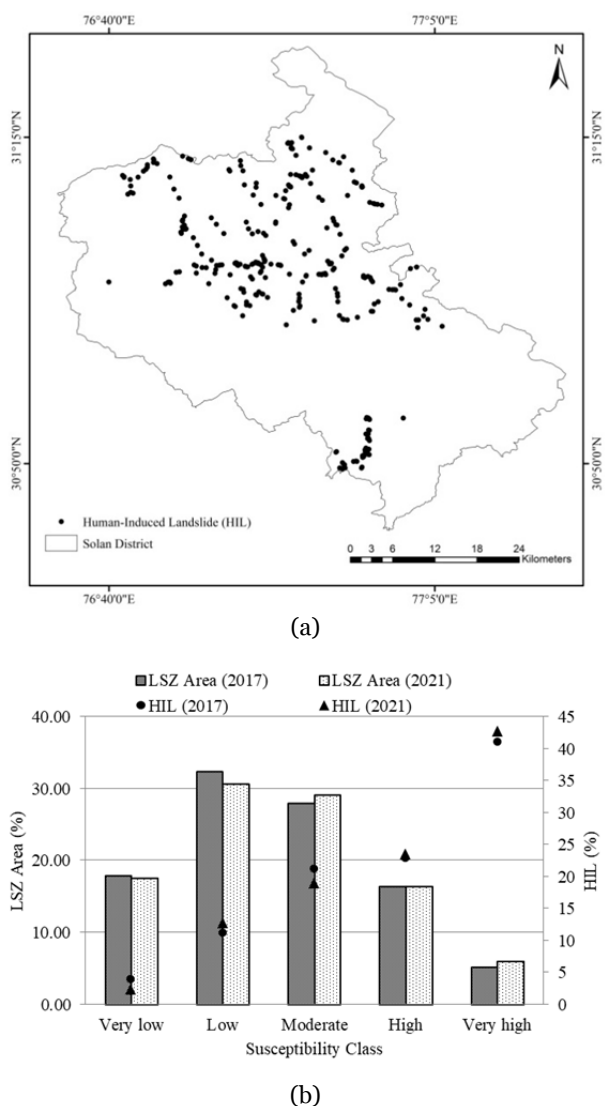


Fig. 11 (a) Human-induced landslide (HIL) distribution in different susceptibility classes; (b) Comparison between landslide susceptibility zonation (LSZ) in 2017 and 2021.

Spatial distribution of landslides has been classified into two categories: Rainfall-induced landslide (RIL) and Human-induced landslide (HIL) based on the triggering parameters. Landslide inventory consists of 1777 landslide pixels, where 80% of current landslide events were randomly selected for LSZ training, whereas 20% were utilized for the model validation goals. Nine landslide causative parameters (slope, aspect, curvature, distance to drainage, distance to lineament, lithology, distance to road, NDVI and land use land cover) were utilized to prepare LSZ map along with landslide inventory, which includes both RIL and HIL. In the context of outputs, LSZ map was

produced and reclassified into five classes based on level of susceptibility. The verification and validation results show that the LSZ map simulated by the FR model showed reasonably good prediction accuracy. The influence of anthropogenic parameters has been illustrated by the spatial distribution of RIL and HIL separately along national highways and land use land cover changes (LULCC) from 2017 to 2021. Results indicate a strong relationship between anthropogenic activities and landslide susceptibility. Key conclusions and findings are as follows:

1. Landslide susceptibility map of the Solan district shows that the entire study area can be divided into five respective susceptibility classes: very low (17.60%), low (30.70%), moderate (29.15%), high (16.48%), and very high (6.07%). Landslide incidences in these classes are 0.57%, 8.11%, 21.57%, 31.39% and 38.36%, respectively. Landslides susceptibility is higher along the road network.

2. For each susceptibility class, the landslide density was computed and it was observed that the landslide density value for the very high susceptible zone is 6.324 and 6.559 for the training and testing dataset, respectively. These values are very close and considerably on the higher side as compared to other susceptible classes.

3. The success rate and prediction rate curves indicate that the AUC for the training and testing dataset are 0.79 & 0.80. Furthermore, the result of RMSE is 0.056. The validation results confirm that the proposed LSZ map has reasonably good predictive capacity.

4. Two LSZ maps were produced and compared using LULC for the years 2017 and 2021 to analyze the effect of anthropogenic activities. Comparison results indicate areas belonging to high susceptible classes have been increased, whereas lower susceptible classes have been reduced.

5. A detailed study along national highways (NH 5, NH 907A, NH 105 and NH 205) indicates that a total of 232 landslides occurred along highways within a 1 km buffer zone. Out of these, more than 50 % are triggered due to anthropogenic parameters.

The proposed study will contribute significantly to the first priority of the latest Sendai Framework (2015 - 2030), which governs and guides the context of disaster risk reduction and disaster resilience internationally. This proposed study will be helpful in disaster risk reduction planning, mitigation measure and future development strategies.

References

- Abancó C, Hürlimann M (2014) Estimate of the debris-flow entrainment using field and topographical data. *Nat hazards* 71:363-383.
<https://doi.org/10.1007/s11069-013-0930-5>
- Abdo HG (2022) Assessment of landslide susceptibility zonation using frequency ratio and statistical index: a case study of Al-Fawar basin, Tartous, Syria. *Int J Environ Sci Technol* 19: 2599-2618.
<https://doi.org/10.1007/s13762-021-03322-1>
- Agarwal PD, Dixit RS (1986) A study of landslides associated with road construction in himalayas. In: Australian Road Research Board (ARRB) Conference, 13th, 1986, Adelaide, Australia.
- Akinci H, Zeybek M (2021) Comparing classical statistic and machine learning models in landslide susceptibility mapping in Ardancuc (Artvin), Turkey. *Nat Hazards* 108: 1515-1543.
<https://doi.org/10.1007/s11069-021-04743-4>
- Akinci H, Zeybek M, Dogan S (2021) Evaluation of landslide susceptibility of Şavşat District of Artvin Province (Turkey) using machine learning techniques. In: *Landslides*. IntechOpen.
<https://doi.org/10.5772/intechopen.99864>
- Al-Najjar HAH, Pradhan B, Kalantar B, et al. (2021) Landslide susceptibility modeling: An integrated novel method based on machine learning feature transformation. *Remote Sens* 13: 3281.
<https://doi.org/10.3390/rs13163281>
- Alsabhan AH, Singh K, Sharma A, et al. (2022) Landslide susceptibility assessment in the Himalayan range based along Kasauli-Parwanoo road corridor using weight of evidence, information value, and frequency ratio. *J King Saud Univ* 34: 101759.
<https://doi.org/10.1016/j.jksus.2021.101759>
- Althuwaynee OF, Pradhan B, Lee S (2016) A novel integrated model for assessing landslide susceptibility mapping using CHAID and AHP pair-wise comparison. *Int J Remote Sens* 37: 1190-1209.
<https://doi.org/10.1080/01431161.2016.1148282>
- Anbalagan R, Kumar R, Lakshmanan K, et al. (2015) Landslide hazard zonation mapping using frequency ratio and fuzzy logic approach, a case study of Lachung Valley, Sikkim. *Geoenvironmental Disasters* 2: 1-17.
<https://doi.org/10.1186/s40677-014-0009-y>
- Anbazhagan VRS (2015) Landslide susceptibility mapping along Kollil hills Ghat road section (India) using frequency ratio , relative effect and fuzzy logic models. *Environ Earth Sci* 8009-8021.
<https://doi.org/10.1007/s12665-014-3954-6>
- Arbanas Ž, Dugonjić S (2010) Landslide risk increasing caused by highway construction. *Proc. of the Interpraevent* 333-343.
- Ayalew L, Yamagishi H (2005) The application of GIS-based logistic regression for landslide susceptibility mapping in the Kakuda-Yahiko Mountains, Central Japan. *Geomorphology* 65: 15-31.
<https://doi.org/10.1016/j.geomorph.2004.06.010>
- Ayalew L, Yamagishi H, Ugawa N (2004) Landslide susceptibility mapping using GIS-based weighted linear combination, the case in Tsugawa area of Agano River, Niigata Prefecture, Japan. *Landslides* 1: 73-81.
<https://doi.org/10.1007/s10346-003-0006-9>
- Basu T, Pal S (2019) A GIS □ based factor clustering and landslide susceptibility analysis using AHP for Gish River Basin , India, Environment, Development and Sustainability. Springer Netherlands.
<https://doi.org/10.1007/s10668-019-00406-4>
- Chen W, Xie X, Wang J, et al. (2017) A comparative study of logistic model tree, random forest, and classification and regression tree models for spatial prediction of landslide susceptibility. *Catena* 151: 147-160.
<https://doi.org/10.1016/j.catena.2016.11.032>
- Chuang YC, Shiu YS (2018) Relationship between landslides and mountain development—Integrating geospatial statistics and a new long-term database. *Sci Total Environ* 622: 1265-1276.
<https://doi.org/10.1016/j.scitotenv.2017.12.039>
- Conoscenti C, Ciaccio M, Caraballo-Arias NA, et al. (2015) Assessment of susceptibility to earth-flow landslide using logistic regression and multivariate adaptive regression splines: a case of the Belice River basin (western Sicily, Italy). *Geomorphology* 242: 49-64.
<https://doi.org/10.1016/j.geomorph.2014.09.020>
- Couture R (2011) Landslide Terminology: National Technical Guidelines and Best Practices on Landslides; Geological Survey of Canada, Open File 6824. *Nat Resour Canada* Ottawa, ON, Canada.
<https://doi.org/10.4095/288066>
- Dai FC, Lee CF (2002) Landslide characteristics and slope instability modeling using GIS, Lantau Island, Hong Kong. *Geomorphology* 42: 213-228.
[https://doi.org/10.1016/S0169-555X\(01\)00087-3](https://doi.org/10.1016/S0169-555X(01)00087-3)
- Ding Q, Chen W, Hong H (2017) Application of frequency ratio, weights of evidence and evidential belief function models in landslide susceptibility mapping. *Geocarto Int* 32: 619-639.
<https://doi.org/10.1080/10106049.2016.1165294>
- Emadodin S, Taheri V, Mohammad Ghasemi M, Nazari Z (2021) Landslide Susceptibility Zonation applying frequency ratio models and statistical index in in Oghan watershed. *Quant Geomorpho Res* 9: 75-95.
<https://doi.org/10.22034/GMPJ.2021.248268.1211>
- Galve JP, Cevasco A, Brandolini P, Soldati M (2015) Assessment of shallow landslide risk mitigation measures based on land use planning through probabilistic modelling. *Landslides* 12: 101-114.
<https://doi.org/10.1007/s10346-014-0478-9>
- Gao X, Chen T, Niu R, Plaza A (2021) Recognition and mapping of landslide using a fully convolutional DenseNet and influencing factors. *IEEE J Sel Top Appl Earth Obs Remote Sens* 14: 7881-7894.
<https://doi.org/10.1109/JSTARS.2021.3101203>
- Gariano SL, Guzzetti F (2016) Landslides in a changing climate. *Earth-Science Rev* 162: 227-252.
<https://doi.org/10.1016/j.earscirev.2016.08.011>
- Gariano SL, Rianna G, Petrucci O, Guzzetti F (2017) Assessing future changes in the occurrence of rainfall-induced landslides at a regional scale. *Sci Total Environ* 596: 417-426.
<https://doi.org/10.1016/j.scitotenv.2017.03.103>
- Gautam S, Adhikari BR, Tian B, et al. (2019) An interaction between landslide and road construction: A case study from Sino-Nepal road corridors, in: AGU Fall Meeting Abstracts. p NH33E-0952.
- Gholami M, Ghachkanlu EN, Khosravi K, Pirasteh S (2019) Landslide prediction capability by comparison of frequency ratio, fuzzy gamma and land slide index method. *J Earth Syst Sci* 128: 1-22.
<https://doi.org/10.1007/s12040-018-1047-8>
- Ghosh JK, Bhattacharya D (2010) Knowledge-based landslide susceptibility zonation system. *J of Comput in Civi Eng* 24(4): 325-334.
- Giuseppe F, Simoni S, Godt JW, et al. (2016) Geomorphological control on variably saturated hillslope hydrology and slope instability. *Water Resour Res* 52: 4590-4607.
<https://doi.org/10.1002/2015WR017626>
- Griffiths DV (2015) Slope stability analysis by finite elements: A guide to the use of Program slope64 32.
- Guillard C, Zezere J (2012) Landslide susceptibility assessment and validation in the framework of municipal planning in Portugal: the case of Loures municipality. *Environ. Manage* 50: 721-735.
<https://doi.org/10.1007/s00267-012-9921-7>

- Huang F, Yao C, Liu W, et al. (2018) Landslide susceptibility assessment in the Nantian area of China: a comparison of frequency ratio model and support vector machine. *Geomatics, Nat Hazards Risk* 9: 919-938. <https://doi.org/10.1080/19475705.2018.1482963>
- Jaboyedoff M, Michoud C, Derron MH, et al. (2018) Human-induced landslides: toward the analysis of anthropogenic changes of the slope environment, in: *Landslides and Engineered Slopes. Experience, Theory and Practice*. CRC Press, pp. 217-232.
- Jones S, Kasthurba AK, Bhagyanathan A, Binoy BV (2021) Impact of anthropogenic activities on landslide occurrences in southwest India: An investigation using spatial models. *J Earth Syst Sci* 130: 1-18. <https://doi.org/10.1007/s12040-021-01566-6>
- Kumar R, Anbalagan R (2015) Landslide susceptibility zonation in part of Tehri reservoir region using frequency ratio, fuzzy logic and GIS. *J Earth Syst Sci* 124: 431-448. <https://doi.org/10.1007/s12040-015-0536-2>
- Kumar V, Gupta V, Jamir I (2018) Hazard evaluation of progressive Pawari landslide zone, Satluj valley, Himachal Pradesh, India. *Nat Hazards* 93: 1029-1047. <https://doi.org/10.1007/s11069-018-3339-3>
- Kundu S, Sharma D, Saha A (2011) Gis-Based Statistical Landslide Susceptibility Zonation: a Case Study in Ganeshganga Watershed, the Himalayas. *Esriindia Com* 1-9. <https://doi.org/10.13140/2.1.2597.6008>
- Liu J, Wu Y, Gao X (2021a) Increase in occurrence of large glacier-related landslides in the high mountains of Asia. *Sci Rep* 11: 1-12. <https://doi.org/10.1038/s41598-021-81212-9>
- Liu T, Chen T, Niu R, Plaza A (2021b) Landslide Detection Mapping Employing CNN, ResNet, and DenseNet in the Three Gorges Reservoir, China. *IEEE J Sel Top Appl Earth Obs Remote Sens* 14: 11417-11428. <https://doi.org/10.1109/JSTARS.2021.3117975>
- Lv L, Chen T, Dou J, Plaza A (2022) A hybrid ensemble-based deep-learning framework for landslide susceptibility mapping. *Int J Appl Earth Obs Geoinf* 108: 102713. <https://doi.org/10.1016/j.jag.2022.102713>
- Magliulo P, Di Lisio A, Russo F, Zelano A (2008) Geomorphology and landslide susceptibility assessment using GIS and bivariate statistics: a case study in southern Italy. *Nat hazards* 47: 411-435. <https://doi.org/10.1007/s11069-008-9230-x>
- Mehrabi M (2022) Landslide susceptibility zonation using statistical and machine learning approaches in Northern Lecco, Italy. *Nat Hazards* 111: 901-937. <https://doi.org/10.1007/s11069-021-05083-z>
- Meneses BM, Pereira S, Reis E (2019) Effects of different land use and land cover data on the landslide susceptibility zonation of road networks. *Nat Hazards Earth Syst Sci* 19: 471-487. <https://doi.org/10.5194/nhess-19-471-2019>
- Merzdorf J (2020) Climate Change Could Trigger More Landslides in High Mountain Asia. *NASA's Goddard Sp. Flight Cent.*
- Meusburger K, Alewell C (2008) Impacts of anthropogenic and environmental factors on the occurrence of shallow landslides in an alpine catchment (Urseren Valley, Switzerland). *Nat Hazards Earth Syst Sci* 8: 509-520. <https://doi.org/10.5194/nhess-8-509-2008>
- Mukherjee M, Sangeeta, Madapala J (2020) Sustainable Infrastructure Development, Risk Perception and Vulnerability Assessment in Indian Himalayan Region, IRDR Working Paper Series. <https://doi.org/10.24948/2020.07>
- Nath RR, Sharma ML, Goswami A, et al. (2021) Landslide susceptibility zonation with special emphasis on tectonic features for occurrence of landslides in Lower Indian Himalaya. *J Indian Soc Remote Sens* 49: 1221-1238. <https://doi.org/10.1007/s12524-020-01285-3>
- Nefeslioglu HA, Duman TY, Durmaz S (2008) Landslide susceptibility mapping for a part of tectonic Kelkit Valley (Eastern Black Sea region of Turkey). *Geomorphology* 94: 401-418. <https://doi.org/10.1016/j.geomorph.2006.10.036>
- Nsengiyumva JB, Luo G, Nahayo L, et al. (2018) Landslide susceptibility assessment using spatial multi-criteria evaluation model in Rwanda. *Int J Environ Res Public Health* 15. <https://doi.org/10.3390/ijerph15020243>
- Ozdemir A, Altural T (2013) A comparative study of frequency ratio, weights of evidence and logistic regression methods for landslide susceptibility mapping: Sultan Mountains, SW Turkey. *J Asian Earth Sci* 64: 180-197. <https://doi.org/10.1016/j.jseae.2012.12.014>
- Panchal S, Shrivastava AK (2022) Landslide hazard assessment using analytic hierarchy process (AHP): A case study of National Highway 5 in India. *Ain Shams Eng J* 13: 101626. <https://doi.org/10.1016/j.asej.2021.10.021>
- Panchal S, Shrivastava AK (2021) A comparative study of frequency ratio, Shannon's entropy and analytic hierarchy process (AHP) models for landslide susceptibility assessment. *ISPRS Int J Geo-Information* 10: 603. <https://doi.org/10.3390/ijgi10090603>
- Pandey VK, Sharma KK, Pourghasemi HR, Bandooni SK (2019) Sedimentological characteristics and application of machine learning techniques for landslide susceptibility modelling along the highway corridor Nahan to Rajgarh (Himachal Pradesh), India. *Catena* 182: 104150. <https://doi.org/10.1016/j.catena.2019.104150>
- Pham BT, Bui DT, Prakash I, Dholakia MB (2017) Hybrid integration of Multilayer Perceptron Neural Networks and machine learning ensembles for landslide susceptibility assessment at Himalayan area (India) using GIS. *Catena* 149: 52-63. <https://doi.org/10.1016/j.catena.2016.09.007>
- Pinyol NM, Alonso EE, Corominas J, Moya J (2012) Canelles landslide: modelling rapid drawdown and fast potential sliding. *Landslides* 9: 33-51. <https://doi.org/10.1007/s10346-011-0264-x>
- Pisano L, Zumpano V, Malek Z, et al. (2017) Variations in the susceptibility to landslides, as a consequence of land cover changes: A look to the past, and another towards the future. *Sci Total Environ* 601: 1147-1159. <https://doi.org/10.1016/j.scitotenv.2017.05.231>
- Pourghasemi HR, Mohammady M, Pradhan B (2012) Landslide susceptibility mapping using index of entropy and conditional probability models in GIS: Safarood Basin, Iran. *Catena* 97: 71-84. <https://doi.org/10.1016/j.catena.2012.05.005>
- Pourghasemi HR, Sadhasivam N, Amiri M, et al. (2021) Landslide susceptibility assessment and mapping using state-of-the-art machine learning techniques. *Nat Hazards* 108: 1291-1316. <https://doi.org/10.1007/s11069-021-04732-7>
- Pradhan B, Lee S (2010) Delineation of landslide hazard areas on Penang Island, Malaysia, by using frequency ratio, logistic regression, and artificial neural network models. *Environ Earth Sci* 60: 1037-1054. <https://doi.org/10.1007/s12665-009-0245-8>
- Pradhan B, Sameen MI, Al-Najjar HAH, et al. (2021) A meta-learning approach of optimisation for spatial prediction of landslides. *Remote Sens* 13: 4521. <https://doi.org/10.3390/rs13224521>
- Pradhan B, Seeni MI, Kalantar B (2017) Performance evaluation and sensitivity analysis of expert-based, statistical, machine learning, and hybrid models for producing landslide susceptibility maps, in: *Laser Scanning Applications in Landslide Assessment*. Springer. pp. 193-232. https://doi.org/10.1007/978-3-319-55342-9_11
- Reichenbach P, Mondini AC, Rossi M (2014) The influence of land use change on landslide susceptibility zonation: the

- Briga catchment test site (Messina, Italy). *Environ. Manage* 54: 1372-1384.
<https://doi.org/10.1007/s00267-014-0357-0>
- Ross M.R.V., McGlynn B.L., Bernhardt E.S. (2016) Deep impact: Effects of mountaintop mining on surface topography, bedrock structure, and downstream waters. *Environ Sci Technol* 50: 2064-2074.
<https://doi.org/10.1021/acs.est.5b04532>
- Saha A, Saha S (2021) Application of statistical probabilistic methods in landslide susceptibility assessment in Kurseong and its surrounding area of Darjeeling Himalayan, India: RS-GIS approach. *Environ Dev Sustain* 23: 4453-4483.
<https://doi.org/10.1007/s10668-020-00783-1>
- Saha AK, Gupta RP, Arora MK (2002) GIS-based landslide hazard zonation in the Bhagirathi (Ganga) valley, Himalayas. *Int J Remote Sens* 23: 357-369.
<https://doi.org/10.1080/01431160010014260>
- Saha AK, Gupta RP, Sarkar I, et al. (2005) An approach for GIS-based statistical landslide susceptibility zonation-with a case study in the Himalayas. *Landslides* 2: 61-69.
<https://doi.org/10.1007/s10346-004-0039-8>
- Sangeeta, Maheshwari BK (2022) Spatial predictive modelling of rainfall-and earthquake-induced landslide susceptibility in the Himalaya region of Uttarakhand, India. *Environ Earth Sci* 81: 1-24.
<https://doi.org/10.1007/s12665-022-10352-6>
- Sangeeta, Maheshwari BK (2019) Earthquake-induced landslide hazard assessment of Chamoli district, Uttarakhand using relative frequency ratio method. *Indian Geotech J* 49: 108-123.
<https://doi.org/10.1007/s40098-018-0334-2>
- Sangeeta, Maheshwari BK, Kanungo DP (2020) GIS-based pre-and post-earthquake landslide susceptibility zonation with reference to 1999 Chamoli earthquake. *J Earth Syst Sci* 129: 1-20.
<https://doi.org/10.1007/s12040-019-1319-y>
- Saranaathan S.E., Mani S., Ramesh V., et al. (2021) Landslide susceptibility zonation mapping using bivariate statistical frequency ratio method and GIS: a case study in part of SH 37 Ghat Road, Nadugani, Panthalur Taluk, The Nilgiris. *J Indian Soc Remote Sens* 49: 275-291.
<https://doi.org/10.1007/s12524-020-01207-3>
- Shahabi H, Khezri S, Ahmad B Bin, Hashim M (2014) Landslide susceptibility mapping at central Zab basin, Iran: A comparison between analytical hierarchy process, frequency ratio and logistic regression models. *Catena* 115: 55-70.
<https://doi.org/10.1016/j.catena.2013.11.014>
- Shano L, Raghuvanshi TK, Meten M (2021) Landslide susceptibility mapping using frequency ratio model: the case of Gamo highland, South Ethiopia. *Arab J Geosci* 14: 1-18.
<https://doi.org/10.1007/s12517-021-06995-7>
- Sharma A, Prakash C (2021) Evaluating the impact of road construction on landslide susceptibility-A case study of Mandi district, Himachal Pradesh, India. *Authorea Prepr*.
<https://doi.org/10.22541/au.162132838.80285009/v1>
- Sharma A, Sur U, Singh P, et al. (2020) Probabilistic landslide hazard assessment using Statistical Information Value (SIV) and GIS techniques: A case study of Himachal Pradesh, India. *Tech Disaster Risk Manag Mitig* 197-208.
<https://doi.org/10.1002/9781119359203.ch15>
- Sharma RK, Mehta BS (2012) Macro-zonation of landslide susceptibility in Garamaura-Swarghat-Gambhar section of national highway 21, Bilaspur District, Himachal Pradesh (India). *Nat Hazards* 60: 671-688.
<https://doi.org/10.1007/s11069-011-0041-0>
- Sifa SF, Mahmud T, Tarin MA, Haque DME (2020) Event-based landslide susceptibility mapping using weights of evidence (WoE) and modified frequency ratio (MFR) model: A case study of Rangamati district in Bangladesh. *Geol Ecol Landscapes* 4: 222-235.
<https://doi.org/10.1080/24749508.2019.1619222>
- Singh P, Sharma A, Sur U, Rai PK (2021) Comparative landslide susceptibility assessment using statistical information value and index of entropy model in Bhanupali-Beri region, Himachal Pradesh, India. *Environ Dev Sustain* 23: 5233-5250.
<https://doi.org/10.1007/s10668-020-00811-0>
- Tanyas H, Gorum T, Kirschbaum D, Lombardo L (2022) Could road constructions be more disastrous than an earthquake in terms of landsliding? *Nat Hazards* 112: 639-663.
<https://doi.org/10.1007/s11069-021-05199-2>
- Thomas AV, Saha S, Danumah JH, et al. (2021) Landslide susceptibility zonation of Idukki district using GIS in the aftermath of 2018 Kerala floods and landslides: A comparison of AHP and frequency ratio methods. *J Geovisualization Spat Anal* 5: 1-27.
<https://doi.org/10.1007/s41651-021-00090-x>
- Tsangaratos P, Ilia I, Hong H, et al. (2017) Applying Information Theory and GIS-based quantitative methods to produce landslide susceptibility maps in Nancheng County, China. *Landslides* 14: 1091-1111.
<https://doi.org/10.1007/s10346-016-0769-4>
- Vakhshoori V, Zare M (2016) Landslide susceptibility mapping by comparing weight of evidence, fuzzy logic, and frequency ratio methods. *Geomatics, Nat Hazards Risk* 7: 1731-1752.
<https://doi.org/10.1080/19475705.2016.1144655>
- Vanacker V, Vanderschaeghe M, Govers G, et al. (2003) Linking hydrological, infinite slope stability and land-use change models through GIS for assessing the impact of deforestation on slope stability in high Andean watersheds. *Geomorphology* 52: 299-315.
[https://doi.org/10.1016/S0169-555X\(02\)00263-5](https://doi.org/10.1016/S0169-555X(02)00263-5)
- Wadadar S, Mukhopadhyay BP (2022) GIS-based landslide susceptibility zonation and comparative analysis using analytical hierarchy process and conventional weighting-based multivariate statistical methods in the Lachung River Basin, North Sikkim. *Nat Hazards* 1-38.
<https://doi.org/10.1007/s11069-022-05344-5>
- Wallemaq P, Below R, McLean D (2018) UNISDR and CRED report: Economic losses, poverty & disasters (1998-2017). CRED, Brussels.
- Wan L, Chen T, Plaza A, Cai H (2021) Hyperspectral unmixing based on spectral and sparse deep convolutional neural networks. *IEEE J Sel Top Appl Earth Obs Remote Sens* 14: 11669-11682.
<https://doi.org/10.1109/JSTARS.2021.3126755>
- Yalcin A, Bulut F (2007) Landslide susceptibility mapping using GIS and digital photogrammetric techniques: a case study from Ardesen (NE-Turkey). *Nat Hazards* 41: 201-226.
<https://doi.org/10.1007/s11069-006-9030-0>